Difference between Powder Bed Density and Green Density for a Free-flowing Powder in Binder Jetting Additive Manufacturing

Ming Li

xaviorsbear2015@tamu.edu

Department of Industrial and Systems Engineering, Texas A&M University, College Station, TX, US

Guanxiong Miao

gm2666@tamu.edu

Department of Mechanical Engineering, Texas A&M University, College Station, TX, US

Wenchao Du

wenchaodu@tamu.edu

Department of Industrial and Systems Engineering, Texas A&M University, College Station, TX, US

Zhijian Pei

zjpei@tamu.edu

Department of Industrial and Systems Engineering, Texas A&M University, College Station, TX, US

Chao Ma*

cma@tamu.edu

Department of Engineering Technology and Industrial Distribution, Texas A&M University, College Station, TX, US

Department of Industrial and Systems Engineering, Texas A&M University, College Station, TX, US

Department of Mechanical Engineering, Texas A&M University, College Station, TX, US

* Corresponding author. E-mail address: cma@tamu.edu. Postal address: 3367 TAMU, College Station, TX 77843-3367, US.

Abstract

In binder jetting additive manufacturing, the final part density is closely related to powder bed density and green density. Though powder bed density is considered one of the most critical factors to control and predict green density, their difference has not been fully understood. In this work, experiments and simulations were employed to investigate their difference for a free-flowing powder in a counter-rotating roller powder spreading system. Using an alumina powder with excellent flowability, both experiments and simulations show that powder bed density is higher than green density. Furthermore, simulations provide an in-depth understanding of the density difference. Specifically, in the powder bed density scenario where particles are able to move across different powder layers, a slower powder flow with a smooth velocity transition is observed. In the green density scenario where powder is spread on a printed powder layer, the confined layer space generates a powder flow with higher velocity and more turbulence. As a result, the powder packing structure in the green density scenario has more void space near layer interface than that in the powder bed density scenario. This paper reports a reason for the difference between powder bed density and green density for the first time.

Keywords: Binder jetting, powder bed density, green density

1 Introduction

In binder jetting additive manufacturing (BJAM), a powder-bed-based process, green parts are printed in a powder bed using a liquid binder and then go through post processing (such as sintering) for densification [1]. BJAM has many advantages over other additive manufacturing technologies, including extensive geometry freedom, minimal support structure requirements, great versatility in materials, high scalability, and low machine cost. In BJAM, the density of green parts (i.e., green density) affects the density and thereby other properties of the final parts.

According to a comprehensive literature review on density [2], a strong positive correlation lies between green density and sintered density. Furthermore, with higher green density, parts will have a lower shrinkage during sintering [3-5]. It has been reported that green density can be affected by the powder properties, the conditions of powder spreading and binder deposition, and the quality of powder bed [5-12].

Powder bed density is the packing density of the powder that has been spread under certain conditions to form a powder bed. Therefore, it has been considered an important factor for forming green parts. Extensive efforts have been made via both numerical simulations [13-25] and experiments [26-32] to investigate the effects of powder properties (e.g., particle size, particle size distribution, and particle shape) and spreading conditions (e.g., spreader geometry, layer thickness, and spreader speeds) on powder bed density. However, there is no reported study that aims to interrogate the difference between green density and powder bed density. The fundamental physics for forming a powder bed with and without printed parts are still unclear. Therefore, it is questionable whether the knowledge about the effects of powder properties and spreading conditions is transferable from powder bed density to green density.

In this study, the difference between green density and powder bed density for a free-flowing powder is investigated by both experiments and simulations. An alumina powder with excellent flowability is used in the study. Green density and powder bed density are experimentally measured by printing cup and solid cube samples on a commercially available binder jetting 3D printer. Discrete element method (DEM) simulations are established for the green density scenario and the powder bed density scenario, respectively, to reveal their different powder spreading mechanisms. For the first time, this paper provides an explanation for how green density is different from powder bed density.

2 Experimental Methods

2.1 Feedstock powder

The alumina powder (#26R-8S70, Inframat, USA) with a nominal particle size of 70 μm was employed in the experiments. Figure 1a shows the micrograph of the powder observed via a scanning electron microscope (SEM, JSM-7500F, JEOL, Japan). The shape of powder particles is highly spherical. The particle size distribution was measured on multiple micrographs taken from different powder samples using ImageJ [33]. As shown in Figure 1b, the alumina powder has a particle size distribution from 15 to 120 μm.

According to the powder properties measured in the previous work [32], the apparent density, tap density, and Hausner ratio of the powder are 52.6%, 60.3%, and 1.15, respectively. Since the alumina powder has such a low Hausner ratio, the flowability of the alumina powder is categorized at the free-flowing level [34]. To minimize the effect of moisture on powder spreading, the alumina powder was dried in an oven at 125 °C for 5 h before each printing process.

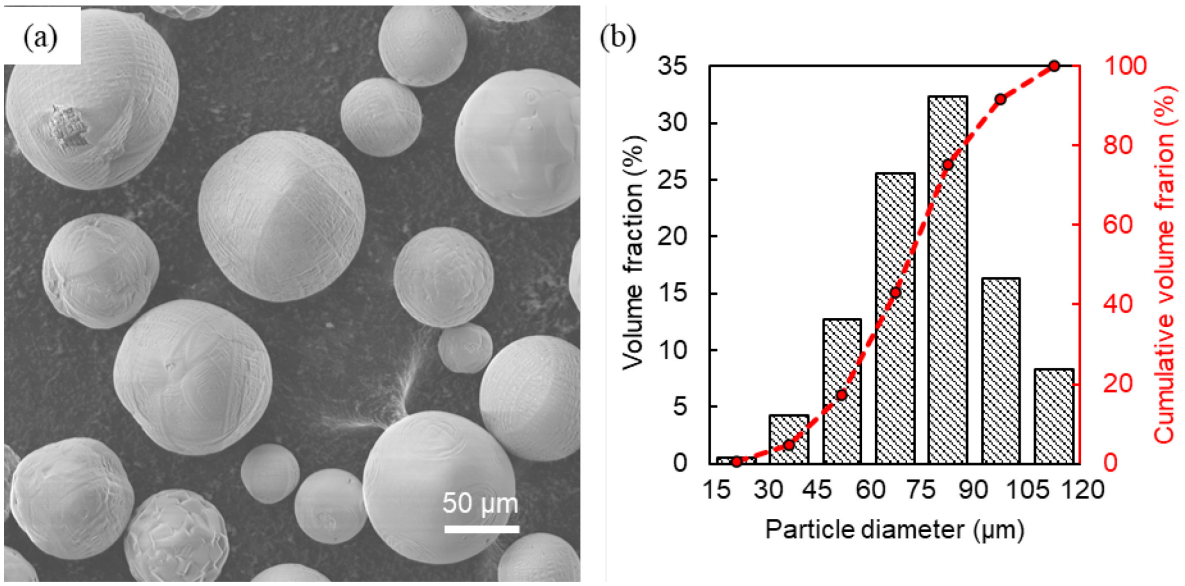

Figure 1. Characterization results of the alumina powder: (a) particle morphology and (b) particle size distribution

2.2 Measurements of powder bed density and green density

Figure 2 shows the design of cup and solid cube samples for measuring powder bed density and green density, respectively. The inner dimensions of the cup are the same as the outer dimensions of the solid cube. To examine and mitigate the influence of surface roughness on volume measurements, all cups and solid cubes were printed with five levels of side length (l), which were 8, 12, 16, 20, and 24 mm. Samples of each level were printed with four replications. The location of the cups and cubes on powder bed was randomized. Additionally, the cavities of the cups were at the same height as the cubes during the printing process.

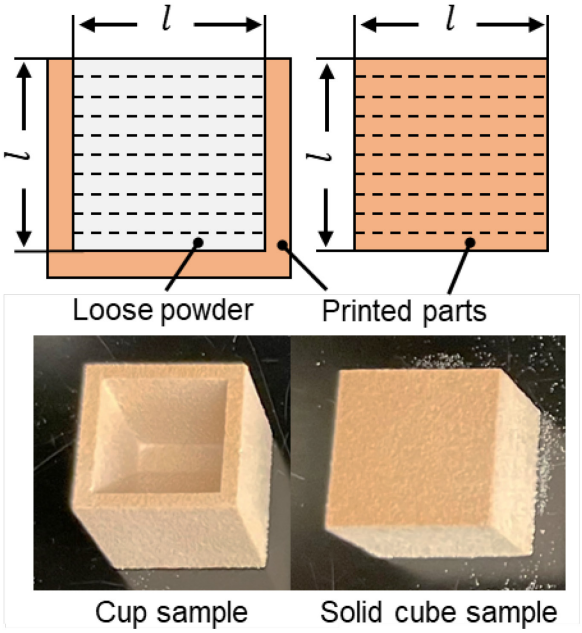

Figure 2. Cup and solid cube samples for measuring powder bed density and green density, respectively

The printing experiments were conducted on a commercially available binder jetting 3D printer (ExOne Innovent+, USA). Table 1 lists the printing parameters. The value of each printing parameter was determined based on some preliminary tests to obtain adequate quality of the

powder bed (e.g., no apparent surface defects) and green samples (e.g., strength and dimensional accuracy).

Table 1. Printing parameters and their values used in the experiments

Parameter	Value
Layer thickness (μm)	160
Roller traverse speed (mm/s)	100
Roller rotational speed (rpm)	500
Binder saturation (%)	35
Bottom bleed reduction	Medium
Binder set time (s)	20
Dry time (s)	13
Ultrasonic mode	A
Ultrasonic intensity (%)	25
Recoat speed (mm/s)	100

After the samples were printed, the whole powder bed was cured at 200 °C for 5 h. The loose powder surrounding the printed samples was then removed by a soft brush. The mass of solid cubes and powder in the cups was measured by a balance with a resolution of 0.001 g. A caliper with a resolution of 0.01 mm was used to measure the outer dimensions of the cubes and the inner dimensions of the cups in order to calculate the corresponding volume. Green density is determined by the mass and volume of the cubes. Powder bed density is determined by the mass of powder contained in the cups and the inner volume of the cups.

3 Numerical Simulation Methods

3.1 Simulation software

The numerical simulations of the powder spreading process were performed using an open-source DEM software called LIGGGHTS [35]. LIGGGHTS offers the capability of particle-scale DEM modeling and simulates the interparticle interactions with predefined contact laws and

physical parameters. The simulation work was conducted in the Texas A&M High Performance Research Computing (HPRC) facilities using one node and eight CPUs.

3.2 Simulation setup and input parameters

The particles in the simulation were modeled in a discrete manner and considered as soft spheres so that their deformation is accounted for in force models. Two types of forces (i.e., gravitational and contact forces) were applied to determine particle motion in the simulation. The contact force between two particles or between a particle and the spreading apparatus was governed by the Hertzian contact model, called "gran model hertz" in LIGGGHTS. Considering the excellent flowability of the alumina powder, it was assumed that the cohesive force between the particles was negligible compared with the gravitational and contact forces. The contact force was composed of a normal component (F_n) and a tangential component (F_t), as shown in Equations 1 and 2, respectively:

$$F_n = k_n \boldsymbol{\delta_{ij}} \cdot \boldsymbol{n} - \gamma_n \boldsymbol{v_{ij}} \cdot \boldsymbol{n} \quad (1)$$

$$F_t = k_t \boldsymbol{\delta_{ij}} \cdot \boldsymbol{t} - \gamma_t \boldsymbol{v_{ij}} \cdot \boldsymbol{t} \quad (2)$$

where k_n and γ_n (k_t and γ_t) are the elastic constant and the viscoelastic damping constant in the normal (tangential) directions, respectively. $\boldsymbol{\delta_{ij}}$ and $\boldsymbol{v_{ij}}$ are the displacement and the relative velocity between two overlapping objects (i and j). $\boldsymbol{n}$ and $\boldsymbol{t}$ are the unit vectors in the normal and tangential directions, respectively.

In the simulation model, the spreading apparatus was scaled down to achieve a reasonable computational time. As shown in Figure 3, the spreading apparatus consisted of a piston as the build platform with a length of 10 mm (x-axis) and a roller with a diameter of 16 mm. Both the build platform and roller were 1 mm (y-axis) in width. A clearance of 200 μm was set between the lowest point of the roller and the top surface of the build platform wall.

The input parameters about the spreading apparatus and feedstock powder are summarized in Table 2. It should be noted that the Young's modulus in the simulations was reduced to match with the timestep as a common treatment in DEM [36]. The friction coefficient and Poisson's ratio of the spreading apparatus and domain boundaries were set to those of stainless steel [37-39] and the properties of the powder in this simulation were set to those of the alumina powder [40, 41]. The powder was generated following the particle size distribution measurement in Figure 1b and discretized into seven particle sizes (i.e., 22.5, 37.5, 52.5, 67.5, 82.5, 97.5, and 119.1 μm).

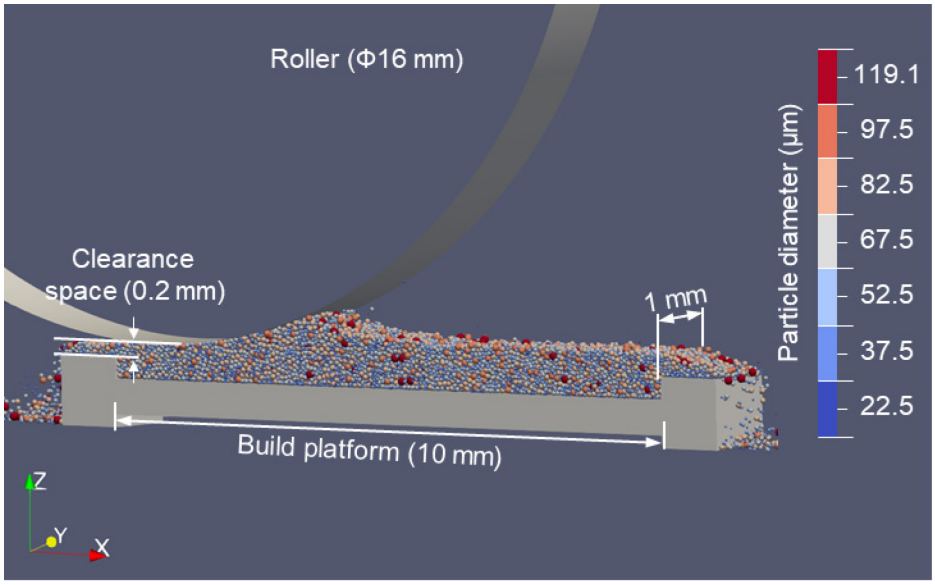

Figure 3. Illustration of the simulation setup

Table 2. Input parameters in the DEM simulations

Parameter	Spreading apparatus	Feedstock powder
Density (kg/m^3)	8050	3970
Young's modulus (Pa)	0.9×10^9	1.0×10^9
Poisson's ratio	0.28	0.23
Friction coefficient	0.15 (*particle-roller*)	0.70 (*particle-particle*)

3.3 Powder spreading scenarios for powder bed density and green density

The powder spreading process was simulated under two different scenarios: powder bed density (PBD) scenario and green density (GD) scenario. In the PBD scenario, powder was spread on a loose layer where particles were able to move freely. In the GD scenario, powder was spread on a printed layer where particles in the printed zone had no mobility. The printed zone was in the center of the powder bed along the x-axis with a length of 8 mm and was across the entire width (y-axis) and height (z-axis) of the previously spread layer(s).

In order to avoid the wall effects from the bottom boundary or top boundary of the powder bed on the density calculation [13], three layers were simulated and the second (middle) layer was used to calculate density. The procedures of the powder spreading process are shown in Figure 4. Before spreading the first layer, in order to fill the clearance between the roller and the build platform surface, the build platform moved downward along the z-axis to create a pocket with a depth equal to the sum of the clearance (200 μm) and the layer thickness (160 μm). Before spreading the second or third layer, the build platform moved downward by a distance of layer thickness (160 μm) instead. The feedstock powder was generated above the build platform and was allowed to freely fall onto the build platform. The total volume of powder deposited on the build platform was 2.5 times that needed to fill the space above the build platform, with both volumes calculated based on the apparent density of the powder. The roller started to spread powder from left to right (along the x-axis) at the same roller traverse speed and roller rotating speed as those used in the experiments (shown in Table 1). When the roller moved beyond the build platform, the powder spreading process was finished and the powder bed was formed.

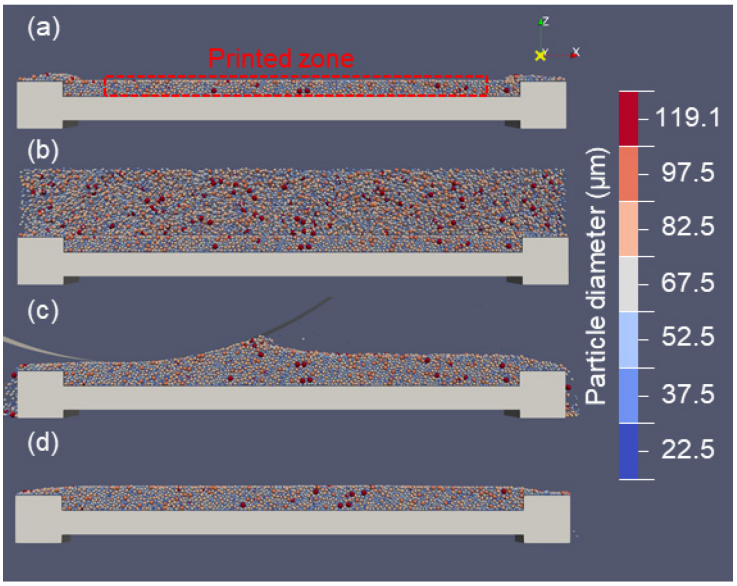

Figure 4. Simulation procedures of the powder spreading process of the second layer as an example: (a) the initial stage (a printed zone in the first layer in the GD scenario is shown); (b) deposition of the new powder; (c) roller moving from left to right (along the x-axis) to spread the powder; and (d) the final stage of spreading the second layer.

4 Results and discussion

4.1 Experimental results

Figure 5 shows powder bed density and green density measured on the printed cup and solid cube samples. The results show that powder bed density is higher than green density for all sample sizes. The mean powder bed density and the mean green density are 59.2% and 52.3%, respectively.

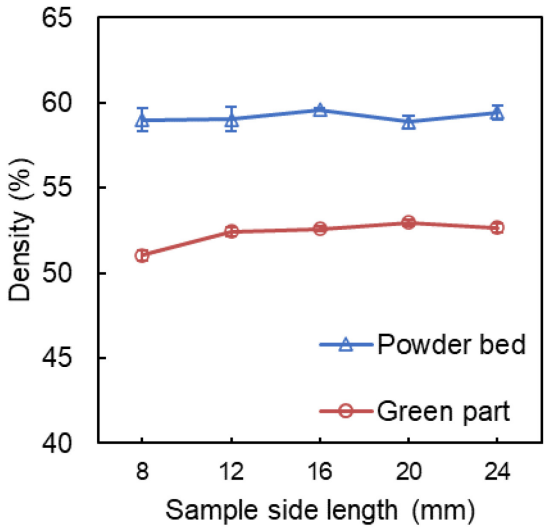

Figure 5. Powder bed density and green density measured on the cup and solid cube samples with different sizes

Similar relationships between green density and powder bed density can be found in the literature. Miyanaji [12] reported that among three stainless steel 316L powders with different particle sizes, the powder with the largest particle size (44–106 μm) exhibited the most significant difference between green density and powder bed density while the difference decreased as the particle size decreased. It is possible that powders with good flowability, such as the alumina powder used in this study and the stainless steel 316L powder with the largest particle size in Miyanaji's study, are prone to lead to a lower green density than powder bed density.

4.2 Simulation results

4.2.1 Powder packing density in different scenarios

Figure 6 shows the powder packing density of the second layer considering the different sampling regions in the PBD and GD scenarios. The packing density was calculated by the ratio of the solid mass of particles contained in the sampling region (including the whole spheres and spherical segments) to the volume of the sampling region. The overall packing density of the entire

second layer obtained in the PBD scenario is higher than that obtained in the GD scenario, which is in consensus with the experimental results described in Section 4.1. In order to further compare the PBD and GD scenarios, the second layer was evenly divided into three sampling regions (i.e., bottom region, middle region, and top region). Figure 6 shows the regional packing densities in these different sampling regions. The regional packing densities obtained in the PBD scenario remain relatively constant across the entire layer (i.e., bottom region, middle region, and top region) while an obvious discrepancy is observed in the GD scenario. The regional packing densities obtained in the PBD scenario are larger than those in the GD scenario, except for the top region. Although the value of top region packing density obtained in the GD scenario is greater than that in the PBD scenario, the bottom region packing density obtained in the GD scenario is much lower.

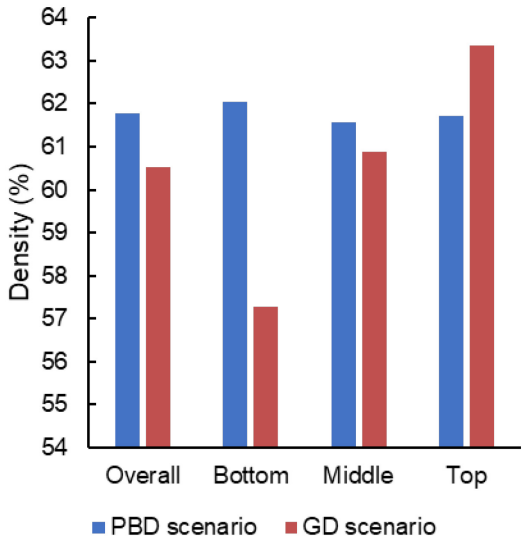

Figure 6. Simulated powder packing density of the second layer considering different sampling regions in the PBD and GD scenarios

The local packing density was further examined by evenly dividing the second layer into sixteen segments with 10 μm in height (along the z-axis). The local packing density of each

segment was calculated by the ratio of the solid mass of particles contained in the sampling region to the volume of the sampling region. As shown in Figure 7, the PBD scenario has similar local packing densities among all segments, with a small standard deviation of 0.38%. However, the local pack densities in the GD scenario show a significant fluctuation, with a much larger standard deviation of 5.43%. The bottom region has the lowest density while the top region has the highest density. The density in the middle region is between those in the bottom and top regions. These results agree with those shown in Figure 6. The significant difference in packing density between the PBD and GD scenarios suggests their differently structured layers, which will be discussed in Section 4.2.2.

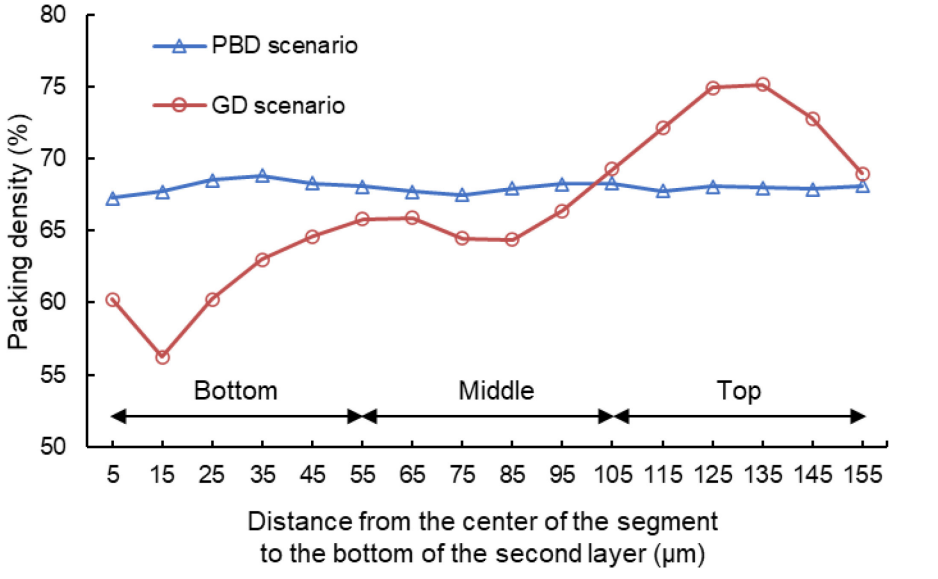

Figure 7. Simulated local packing density in each small segment (10 μm in height) in the PBD and GD scenarios

4.2.2 Powder packing structure in different scenarios

The powder packing structures were captured after the roller exited the powder bed for 0.03 s to let all particles settle sufficiently. Figure 8 shows the horizontal cross sections (parallel to the x-y plane) of exemplary segments in the top and bottom regions of the powder bed in the PBD and

GD scenarios. More specifically, the two segments that are 15 and 135 μm from the bottom of the second layer, respectively, are selected (i.e., thesecond and forthteenth segments from the left in Figure 7). The powder packing structures in the PBD scenario are very similar between the top and bottom regions in Figures 8a and 8b and those in the GD scenario are clearly different in Figures 8c and 8d. Comparing the powder packing structures in the bottom region between the two different scenarios, Figures 8a and 8c show the GD scenario has more void space than the PBD scenario. On the contrary, the GD scenario shows a more densely packed structure than the PBD scenario in the top region, as shown in Figures 8b and 8d. These powder packing structures agree with the quantitative results in Figure 7.

Figure 8. Horizontal cross sections (parallel to the x-y plane) of simulated powder packing structure in the PBD scenario (a) in the bottom region and (b) in the top region of the second layer, and in the GD scenario (c) in the bottom region and (d) in the top region of the second layer

The vertical cross sections (parallel to the x-z plane) of the powder bed in both PBD and GD scenarios are shown in Figure 9, where layer interfaces are marked by the orange dashed lines. To better illustrate the difference in the powder packing structures, magnified powder bed cross sections are also shown. In the PBD scenario, a relatively uniform powder bed is observed across the three layers. In the GD scenario, particles near the layer boundaries tend to align with the layer interfaces. In addition, there is more void space present within the second layer in the GD scenario, especially in the areas close to the bottom of the layer as discussed in Figures 7 and 8. One of the reasons could be that the previous layer restricts the free movement of particles and impedes

particles to pack effectively. Therefore the volume of void space is higher right above the layer interface.

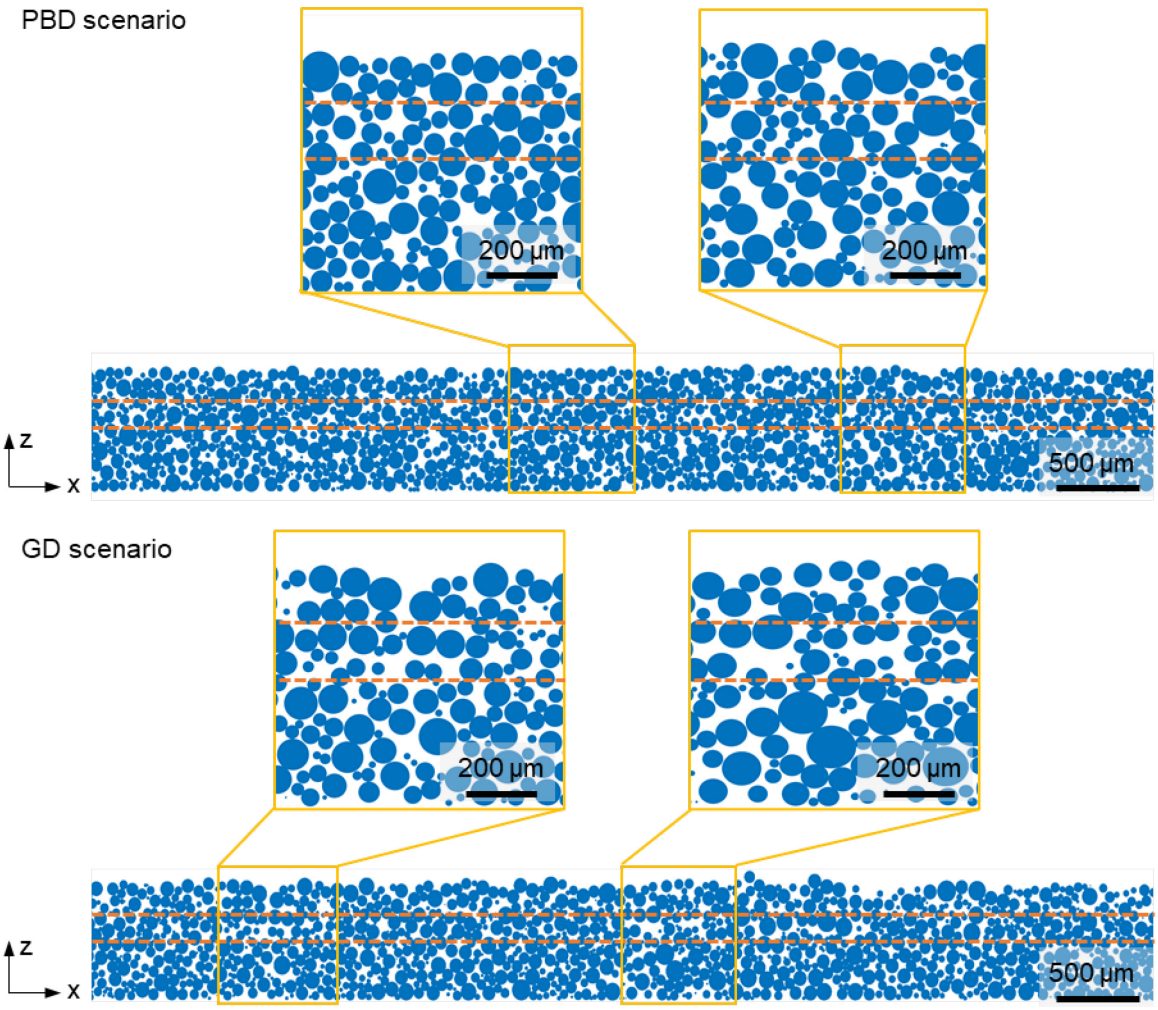

Figure 9. Vertical cross sections (parallel to the x-z plane) of simulated powder packing structure in the PBD and GD scenarios (note: orange dashed lines represent the interfaces between layers)

4.2.3 Powder flowing behaviors in different scenarios

For a deeper understanding of the difference between the PBD and GD scenarios, powder flowing behaviors were studied. As shown in Figure 10, the particle velocity fields in both PBD and GD scenarios were captured at the same timestep during spreading the third layer. Both the magnitude and direction of particle velocity were plotted. Noticeably, distinct flowing behaviors

are present in the PBD and GD scenarios. The PBD scenario has a smooth velocity transition between the new layer and the previously spread layers. The layer interface in the GD scenario hinders the powder flow from further transferring to deeper (the negative direction along the z-axis) and further (the positive direction along the x-axis) regions in the powder bed, and therefore increases particle velocity and generates more turbulence.

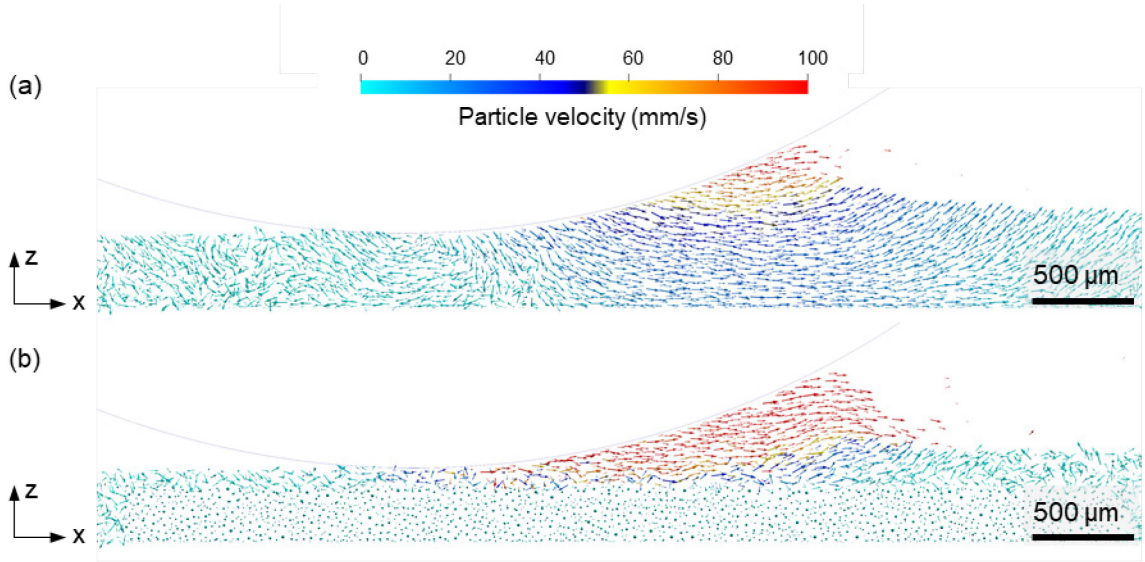

Figure 10. Simulated particle velocity field (a) in the PBD scenario and (b) in the GD scenario

The difference in the powder packing structures between the PBD and GD scenarios is a consequence of how particles from the newly spread layer interact with those from the layers underneath. The particle rearrangement space determines the extent of powder mixing during spreading. In the PBD scenario, the high packing density can be achieved because of the sufficient powder mixing among a large number of particles across different layers. In the GD scenario, powder mixing is less effective owing to the limited layer space for free movement of particles. Impacted by the layer interface, particles in the newly spread layer are difficult to be distributed as uniformly and packed as densely as those in the PBD scenario.

5 Conclusions

Using both experimental and numerical approaches, this study provides insights into the difference between powder bed density and green density for a free-flowing powder in binder jetting additive manufacturing. Their difference was studied as a result of how the new layer is spread, namely, spreading on a loose layer in the powder bed density (PBD) scenario or spreading on a printed layer in the green density (GD) scenario. Powder packing structures and powder flowing behaviors were investigated to reveal the underlying mechanisms. The following findings are obtained in this study:

1) In the experiments, the measured powder bed density is higher than the measured green density.
2) The simulated density results agree well with the experimental measurements.
3) The packing density obtained in the PBD scenario remains relatively consistent across a layer while an obvious density variation is observed in the GD scenario.
4) The simulations reveal that the PBD scenario obtains a relatively uniform structure. The GD scenario has more void space near the powder bed surface and near the layer interface area than the PBD scenario.
5) The simulations also reveal that the powder flow during spreading in the PBD scenario tends to transfer deeper and further in the powder bed than that in the GD scenario. The powder movements in the GD scenario are confined by the previously printed layer and thus more turbulence is generated in its powder flow. As a result, the GD scenario obtains a less densely packed powder structure and a lower packing density than PBD scenario.

Declaration of Competing Interest

The authors declare that they have no known competing financial interests or personal relationships that could have appeared to influence the work reported in this paper.

Acknowledgement

This material is based upon work supported by the National Science Foundation (Grant No. 1762341).

References

[1] Standard terminology for additive manufacturing technologies, ASTM International F2792-12a, 2012.

[2] W. Du, X. Ren, Z. Pei, C. Ma, Ceramic binder jetting additive manufacturing: a literature review on density. Journal of Manufacturing Science and Engineering, 142(4) (2020) 040801.

[3] M. Li, W. Du, A. Elwany, Z. Pei, C. Ma, Metal binder jetting additive manufacturing: a literature review, Journal of Manufacturing Science and Engineering 142(9) (2020) 090801.

[4] M. Ziaee, N.B. Crane, Binder jetting: A review of process, materials, and methods, Additive Manufacturing 28 (2019) 781-801.

[5] E. Wheat, M. Vlasea, J. Hinebaugh, C. Metcalfe, Sinter structure analysis of titanium structures fabricated via binder jetting additive manufacturing, Materials & Design 156 (2018) 167-183.

[6] H. Miyanaji, N. Momenzadeh, L. Yang, Effect of powder characteristics on parts fabricated via binder jetting process, Rapid Prototyping Journal 25(2) (2019) 332-342.

[7] I. Rishmawi, M. Salarian, M. Vlasea, Tailoring green and sintered density of pure iron parts using binder jetting additive manufacturing, Additive Manufacturing 24 (2018) 508-520.

[8] H. Miyanaji, K.M. Rahman, M. Da, C.B. Williams, Effect of fine powder particles on quality of binder jetting parts, Additive Manufacturing 36 (2020) 101587.

[9] B. Barthel, F. Janas, S. Wieland, Powder condition and spreading parameter impact on green and sintered density in metal binder jetting, Powder Metallurgy 64(5) (2021) 378-386.

[10] Y. Bai, G. Wagner, C.B. Williams, Effect of bimodal powder mixture on powder packing density and sintered density in binder jetting of metals, International Solid Freeform Fabrication Symposium, Austin, TX, USA, 2015, pp. 758-771.

[11] S. Cao, Y. Qiu, X.-F. Wei, H.-H. Zhang, Experimental and theoretical investigation on ultra-thin powder layering in three dimensional printing (3DP) by a novel double-smoothing mechanism, Journal of Materials Processing Technology 220 (2015) 231-242.

[12] H. Miyanaji, Binder jetting additive manufacturing process fundamentals and the resultant influences on part quality, Ph.D. Disseratation, University of Louisville, 2018.

[13] H. Chen, Q. Wei, Y. Zhang, F. Chen, Y. Shi, W. Yan, Powder-spreading mechanisms in powder-bed-based additive manufacturing: Experiments and computational modeling, Acta Materialia 179 (2019) 158-171.

[14] Y.M. Fouda, A.E. Bayly, A DEM study of powder spreading in additive layer manufacturing, Granular Matter 22(1) (2020) 1-18.

[15] S. Haeri, Optimisation of blade type spreaders for powder bed preparation in additive manufacturing using DEM simulations, Powder Technology 321 (2017) 94-104.

[16] S. Haeri, Y. Wang, O. Ghita, J. Sun, Discrete element simulation and experimental study of powder spreading process in additive manufacturing, Powder Technology 306 (2017) 45-54.

[17] Y. He, A. Hassanpour, A.E. Bayly, Linking particle properties to layer characteristics: Discrete element modelling of cohesive fine powder spreading in additive manufacturing, Additive Manufacturing 36 (2020) 101685.

[18] W. Nan, M. Pasha, T. Bonakdar, A. Lopez, U. Zafar, S. Nadimi, M. Ghadiri, Jamming during particle spreading in additive manufacturing, Powder Technology 338 (2018) 253-262.

[19] W. Nan, M. Pasha, M. Ghadiri, Numerical simulation of particle flow and segregation during roller spreading process in additive manufacturing, Powder Technology 364 (2020) 811-821.

[20] E.J. Parteli, T. Pöschel, Particle-based simulation of powder application in additive manufacturing, Powder Technology 288 (2016) 96-102.

[21] D. Yao, X. An, H. Fu, H. Zhang, X. Yang, Q. Zou, K. Dong, Dynamic investigation on the powder spreading during selective laser melting additive manufacturing, Additive Manufacturing 37 (2021) 101707.

[22] D. Yao, X. Liu, J. Wang, W. Fan, M. Li, H. Fu, H. Zhang, X. Yang, Q. Zou, X. An, Numerical insights on the spreading of practical 316 L stainless steel powder in SLM additive manufacturing, Powder Technology 390 (2021) 197-208.

[23] J. Zhang, Y. Tan, T. Bao, Y. Xu, X. Xiao, S. Jiang, Discrete element simulation of the effect of roller-spreading parameters on powder-bed density in additive manufacturing, Materials 13(10) (2020) 2285.

[24] Y. Lee, A.K. Gurnon, D. Bodner, S. Simunovic, Effect of particle spreading dynamics on powder bed quality in metal additive manufacturing, Integrating Materials and Manufacturing Innovation 9(4) (2020) 410-422.

[25] K. Marchais, J. Girardot, C. Metton, I. Iordanoff, A 3D DEM simulation to study the influence of material and process parameters on spreading of metallic powder in additive manufacturing, Computational Particle Mechanics 8(4) (2021) 943-953.

[26] U. Ali, Y. Mahmoodkhani, S.I. Shahabad, R. Esmaeilizadeh, F. Liravi, E. Sheydaeian, K.Y. Huang, E. Marzbanrad, M. Vlasea, E. Toyserkani, On the measurement of relative powder-bed compaction density in powder-bed additive manufacturing processes, Materials & Design 155 (2018) 495-501.

[27] G. Jacob, A. Donmez, J. Slotwinski, S. Moylan, Measurement of powder bed density in powder bed fusion additive manufacturing processes, Measurement Science and Technology 27(11) (2016) 115601.

[28] G. Jacob, G. Jacob, C.U. Brown, A. Donmez, The influence of spreading metal powders with different particle size distributions on the powder bed density in laser-based powder bed fusion processes, National Institute of Standards and Technology (2018).

[29] N. Karapatis, G. Egger, P. Gygax, R. Glardon, Optimization of powder layer density in selective laser sintering, International Solid Freeform Fabrication Symposium, Austin, Texas, USA, 1999.

[30] K.J. Seluga, Three dimensional printing by vector printing of fine metal powders, Masters' Thesis, Massachusetts Institute of Technology, 2001.

[31] J. Whiting, J. Fox, Characterization of feedstock in the powder bed fusion process: sources of variation in particle size distribution and the factors that influence them, International Solid Freeform Fabrication Symposium, Austin, Texas, USA, 2016.

[32] M. Li, G. Miao, M. Moghadasi, Z. Pei, C. Ma, Ceramic binder jetting additive manufacturing: relationships among powder properties, feed region density, and powder bed density, Ceramics International 47(17) (2021) 25147-25151.

[33] J. Schindelin, I. Arganda-Carreras, E. Frise, V. Kaynig, M. Longair, T. Pietzsch, S. Preibisch, C. Rueden, S. Saalfeld, B. Schmid, Fiji: an open-source platform for biological-image analysis, Nature Methods 9(7) (2012) 676-682.

[34] D. Barletta, M. Poletto, A. Santomaso, Bulk powder flow characterisation techniques, Powder Flow, Royal Society of Chemistry Cambridge, UK, 2019, pp. 64-146.

[35] C. Kloss, C. Goniva, A. Hager, S. Amberger, S. Pirker, Models, algorithms and validation for opensource DEM and CFD–DEM, Progress in Computational Fluid Dynamics, an International Journal 12(2-3) (2012) 140-152.

[36] C. Meier, R. Weissbach, J. Weinberg, W.A. Wall, A.J. Hart, Modeling and characterization of cohesion in fine metal powders with a focus on additive manufacturing process simulations, Powder technology 343 (2019) 855-866.

[37] G. Carter, R. Hooper, J. Henshall, M. Guillou, Friction of metal sliders on toughened zirconia ceramic between 298 and 973 K, Wear 148(1) (1991) 147-160.

[38] S. Howard, Materials Data Book 2003 Edition, Cambridge University Engineering Department, Cambridge, UK, 2003.

[39] J. Song, J.-C. Gelin, T. Barriere, B. Liu, Experiments and numerical modelling of solid state sintering for 316L stainless steel components, Journal of Materials Processing Technology 177(1-3) (2006) 352-355.

[40] B. Bhushan, Modern Tribology Handbook, CRC Press, 2000.

[41] D. Munz, T. Fett, Ceramics: Mechanical Properties, Failure Behaviour, Materials Selection, Springer Science & Business Media, 1999.